^{17}O NMR evidence for vanishing of magnetic polarons in the paramagnetic phase of ceramic $CaMnO_3$

S. Verkhovskii,[1,2] A. Trokiner,[1] A. Gerashenko,[1,2] A. Yakubovskii,[1,3] N. Medvedeva,[4] Z. Litvinova,[2] K. Mikhalev,[2] and A. Buzlukov[2]

[1]*LPEM UPR5, ESPCI ParisTech, CNRS, 75005 Paris, France*

[2]*Institute of Metal Physics, Ural Branch, Russian Academy of Sciences, 620041 Ekaterinburg, Russia*

[3]*Russian Research Centre "Kurchatov Institute," 123182 Moscow, Russia*

[4]*Institute of Solid State Chemistry, Ural Branch, Russian Academy of Sciences, 620018 Ekaterinburg, Russia*

(Received 10 December 2009; revised manuscript received 18 March 2010; published 14 April 2010)

An ^{17}O NMR study of the distribution of the spin and charge densities of a lightly electron-doped $CaMnO_{3-x}$ ($x<0.01$, $T_N=123$ K) ceramic in the paramagnetic phase up to $T=670$ K is reported. The isotropic and anisotropic components of the NMR line shift probe selectively the local spin susceptibility of the itinerant (e_g) and the localized (t_{2g}) electrons of the Mn neighbors whereas the nuclear quadrupole parameters look at the distribution of the charge density along the Mn-O bond. When approaching T_N, the spin density of the doped electrons becomes inhomogeneously distributed: a separation into slow carriers, forming magnetic polarons, and fast carriers develops few tens of degrees above T_N. The energy barrier corresponding to the change in carriers mobility was estimated to ~1100 K. The spin and valence charge densities at the oxygen ions were also measured. From the comparison of these data, the ground state of $CaMnO_3$ appears as a charge-transfer insulator state.

DOI: 10.1103/PhysRevB.81.144415 PACS number(s): 75.47.Lx, 76.60.Es, 76.60.Jx

I. INTRODUCTION

Among the forefront issues of strongly correlated materials are the intriguing inhomogeneities in doped manganese oxides. Ferromagnetic (FM) nanosize domains frozen in the antiferromagnetic (AF) lattice are considered as an intrinsic property of the magnetic ground state of the parent AF insulators lightly doped with holes[1,2] or with electrons.[3–5] In the case of the lightly hole-doped $LaMnO_3$, it was established that these FM entities remain in the whole range of the orbital ordered paramagnetic (PM) phase as small-size FM-dressed polarons with spin and charge fluctuations.[6]

For the lightly electron-doped counterparts, the existence in the AF lattice of small FM domains was confirmed by both a small-angle elastic neutron scattering[7] investigation of $Ca_{1-x}La_xMnO_3$ ($x=0.02$) and a ^{17}O NMR study of $CaMnO_{3-x}$ ($x<0.01$).[8] According to ^{17}O NMR, a nearly perfect alignment of the Mn spins is formed in the FM domains. The static and dynamic properties of these domains agree with the model of a small-size magnetic polaron (MP) for which the FM dressing of the trapped electron is mainly stabilized by the exchange interaction with the core (t_{2g}) spins of the Mn^{4+} ion.[9] The MP starts to move above 40 K in a slow-diffusion regime.

In the PM phase of lightly electron-doped $CaMnO_3$, some clues indicate that the MPs character substantially changes. Indeed, electrical resistivity,[4,10] Hall mobility,[11] thermal conductivity,[12] electron paramagnetic resonance, and Raman-scattering studies[13] are consistent with the large (continuum) polaron theory[14] in contrast with the model of small-polaron hopping for the hole-doped case.

In this paper, we present a ^{17}O NMR study in the PM phase up to 670 K of a lightly electron-doped $CaMnO_{3-x}$ sample ($x<0.01$). We focus on the charge and spin densities transferred to oxygen from Mn ions. The reduced carrier concentration in $CaMnO_{3-x}$ allows tracing with temperature all the components, isotropic and anisotropic, of the ^{17}O NMR line shift. This enables to study the role of the mobile e_g and core t_{2g} electrons through the hyperfine magnetic fields responsible for the ^{17}O line shifts. The hyperfine magnetic shift components show that in the PM phase when approaching T_N, an increasing fraction of mobile e_g electrons becomes FM dressed. In the same temperature range, the spin-echo decay-rate data confirm that these dressed electrons appear with a slower motion.

II. EXPERIMENTAL DETAILS

A polycrystalline sample $CaMnO_{3-x}$ ($x<0.01$) was prepared and then crushed into a coarse-grained (~15 μm) powder for ^{17}O enrichment as described in Ref. 8. The enrichment conditions follow the procedures of Refs. 16 and 17 to obtain a $CaMnO_{3-x}$ with $x<0.02$ composition. The powder was enriched up to ~15% ^{17}O by conditioning at 930 °C during 140 h in an oxygen gas flow ($P_{O_2}\approx 1.5$ bar) with a subsequent slow cooling with the furnace. During the procedure, the thermodynamic equilibrium was controlled and the mass saturation of the powder was achieved within several hours.

As shown by our room-temperature powder x-ray diffraction data, the sample is almost single phase with an orthorhombic structure. The unit-cell parameters determined in the *Pnma* space group are $a=0.52786(6)$ nm, $b=0.74508(10)$ nm, and $c=0.52670(6)$ nm. These values are in the range of the values quoted for a nearly stoichiometric $CaMnO_{3-x}$ ($x<0.01$).[15,16,18–20] Furthermore, the low-temperature magnetization data of this sample presented in Ref. 8 gave an estimate of the O-vacancies content with an upper limit $x=0.01$ that is consistent with the x-ray result.

The well-resolved quadrupole fine structure of ^{17}O NMR spectra discussed in the text shows that the number of ^{17}O nuclei located in grains boundary which are characterized by local structural and charge imperfections[21] represent a negligible fraction ($<10^{-2}$) of the total amount of ^{17}O nuclei in the sample. Thus the NMR data analyzed in this study correspond to nuclei in the bulk for which there is no effect of grain boundaries.

The ^{17}O NMR measurements were performed with ASX BRUKER spectrometers in the temperature range 100–670 K in magnetic fields H_0=70, 94, and 117.4 kOe. The elevated temperature data were acquired with a high-temperature BRUKER probe. Each broad spectrum was obtained by summing the Fourier-transformed half-echo signals acquired at equidistant operating frequencies. The ^{17}O NMR signal in H_2O was used as a frequency reference $\nu_0 = {}^{17}\gamma H_0$ for the shift of NMR line.

In $CaMnO_3$, the ^{17}O resonance frequency is determined by both the quadrupolar interaction ($^{17}I=5/2$; with a quadrupole moment $^{17}Q=-0.02578\times10^{-24}$ cm^2) and the magnetic hyperfine interaction. The simulation of the spectra obtained at different magnetic fields allows one to determine the magnetic shift components $\{K_\alpha\}$ as well as the quadrupole frequency $\nu_Q=[3eQ/2I(2I-1)h]V_{ZZ}$ and asymmetry parameter $\eta=|V_{XX}-V_{YY}|/V_{ZZ}$ of the electric field gradient (EFG) tensor $\{V_{ii}\}$. The powder pattern simulation program takes into account the quadrupole coupling corrections up to the second order in ν_Q/ν_0.

The ^{17}O spin-echo decay rate, T_2^{-1}, was measured on the central peak of ^{17}O NMR spectrum. The echo-decay data were collected using a conventional $\pi/2$-t-π-t-echo pulse sequence. The characteristic time of the echo decay, T_2, is defined as the time at which the echo signal $E(2t)$ drops to $1/e$ of its starting value.

III. RESULTS AND DISCUSSION

A. Electric field gradient at O sites

In the orthorhombic structure of $CaMnO_3$ schematically shown in Fig. 1, the oxygen atoms occupy two sites O(1) and O(2) with a slightly different Mn-O-Mn chemical bond angle, 154(2)°—for O1 site and 157(2)°—for O2 as obtained from our x-ray data and the atomic positions of Ref. 19. The ^{17}O NMR spectrum of the polycrystalline $CaMnO_3$ sample shown in Fig. 1(a) displays a well-resolved quadrupole structure of $2I=5$ peaks corresponding to the transitions $m_I \leftrightarrow m_I-1$. In the case of significantly different spin and charge environments at O(1) and O(2) sites, two sets of parameters $\{K_i\}$ and $\{\nu_Q;\eta\}$ would be required for the spectrum simulation. Remarkably, we obtained that a single set of parameters is enough for a good spectrum simulation within the whole temperature range [Fig. 1(b)].

In order to understand this result, we calculated the quadrupole parameters for both oxygen sites using the point-charge model and *ab initio* full-potential linear augmented plane-wave (FLAPW) method,[22] where the EFG components are determined directly from the charge density as the second derivatives of electrostatic potential at nucleus. The parameters calculated in both approaches are shown in Table I. In

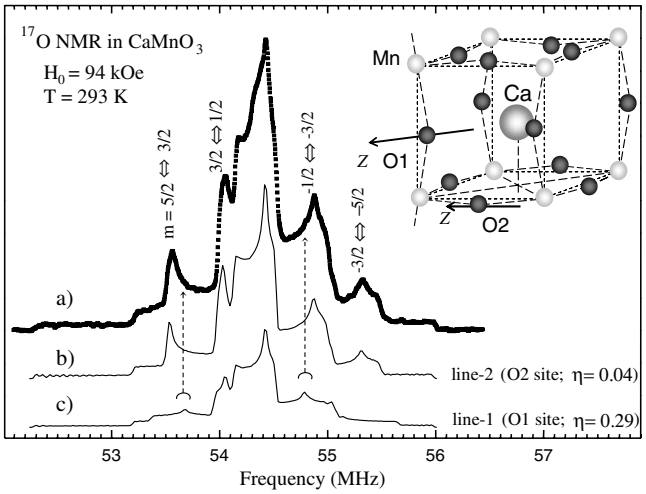

FIG. 1. ^{17}O NMR powder spectrum including all $m_I \leftrightarrow m_I-1$ transitions in $CaMnO_{3-x}$ (a) measured at H=94 kOe, (b) and (c) calculated at O2 and O1 sites, respectively (see text for the EFG parameters used). In the upper corner, the orthorhombic structure is schematically represented with the EFG principal axis, Z, shown by arrows at O1 and O2 oxygen sites.

the point-charge model, the ion charges corresponded to $Ca^{+2}Mn^{+4}O_3^{-2}$ and the Mn^{+4}-O^{-2}-Mn^{+4} bonding are completely ionic. The Sternheimer antishielding factor, $^{17}\gamma_\infty(O^{-2})=-13.785$, was taken from Ref. 23. We took our room-temperature lattice parameters a, b, and c while the atomic positions $\{x/a;y/b;z/c\}$ were taken from Ref. 19. The quadrupolar frequencies obtained in point-charge model [ν_Q=2.8 MHz and 3.3 MHz for the O(1) and O(2) sites, respectively] are much larger than the experimental value $\nu_{Q\,\mathrm{exp}}$=0.937 MHz. *Ab initio* calculations performed for the lattice parameters and atomic coordinates from Ref. 19 [denoted as *Ab initio* (I) in Table I], give ν_Q of 0.86 MHz and 0.875 MHz for O(1) and O(2) sites, respectively. These two values are almost equal and close to $\nu_{Q\,\mathrm{exp}}$. Thus, *ab initio* approach provides much better agreement with experiment than the point-charge model and demonstrates that the covalent effects cannot be ignored for the Mn-O-Mn bonds in perovskites.[24]

In the point-charge model, the asymmetry parameter was calculated to be 0.29 and 0.02 for the O(1) and O(2) sites, respectively, whereas in the *ab initio* calculation, it is 0.29 and 0.08 for the O(1) and O(2) sites, respectively. Both calculations yield the different values for the two oxygen sites. Furthermore, the large value of 0.29 for the O(1) site is inconsistent with our experimental data as shown in Fig. 1(c), where a simulated spectrum for the O(1) site with the parameters $\nu_{Q\,\mathrm{exp}}$=0.937 MHz and η=0.29 is displayed. The two vertical arrows show the singularities which are not detected in the experimental spectra. As already mentioned, there is no indication of grain-boundary effects[21] in the spectra. ^{17}O nuclei close to these grain boundaries should be sensitive to local structural and charge imperfections. In the case where the proportion of these ^{17}O nuclei close to the grain surface is significant, it should result in an EFG distribution which in turn smears the $(m_I \leftrightarrow m_I-1)$ peaks of the spectrum. As shown in Fig. 1(a), this is not our case since the peaks of the spectrum are narrow.

TABLE I. Quadrupolar frequency ν_Q, asymmetry parameter η, and β, the angle between the EFG principal axis ***OZ*** and the edge of the pseudocubic unit cell, calculated in the point-charge model and *ab initio* FLAPW method at O1 and O2 sites in the orthorhombic (*Pnma*) phase of $CaMnO_3$. The sets of lattice parameters and atomic positions utilized in the calculations are explained in the text.

EFG calculation		Point-charge model	*Ab initio* (I)	*Ab initio* (II)
Lattice parameters (nm)	a	0.52786(6)	0.52770(5)	0.52786(6)
	b	0.74508(10)	0.74510(4)	0.74508(10)
	c	0.52670(6)	0.52643(2)	0.52670(6)
Atomic positions $\{x/a;y/b;z/c\}$	Ca(4c)	{0.0272; 0.25; −0.007}		{0.04204; 0.25; −0.0069}
	O1(4c)	{0.487; 0.25; 0.085}		{0.4855; 0.25; 0.0744}
	O2(8d)	{0.289; 0.023; −0.289}		{0.2924; 0.0381; −0.2932}
O1 site	ν_Q (MHz)	2.8	0.860	0.885
	η	0.29	0.29	0.19
	β (deg)	5.5	12	17
O2 site	ν_Q (MHz)	3.3	0.875	0.880
	η	0.02	0.084	0.12
	β (deg)	0.9	0.2	3.6

The EFG asymmetry parameter η is very sensitive to the atomic parameters. Our calculations demonstrate that the atomic O(1) and O(2) positions with coordinates from Ref. 19 retain substantial elastic strains in the $CaMnO_3$ crystal lattice yielding a too large value of η at the O(1) site. We performed the optimization of atomic positions keeping fixed our room-temperature lattice parameters and found that Ca, O1, and O2 are shifted along x, y, and z directions, respectively, by about 0.01 nm [the optimized atomic positions and the EFG parameters are listed in Table I, column denoted as *Ab initio* (II)]. There is almost no change for the two values of ν_Q while the asymmetry parameter changes significantly being much closer for both oxygen sites. The *ab initio* calculations show that the EFG parameters are very similar for both oxygen sites that explains why the O(1) and O(2) sites are hardly distinguished in the experimental spectra of a powder sample. Since there are twice more O(2) sites than the O(1) sites, we believe that our single set of NMR parameters is more relevant to describe the O(2) sites.

With decreasing temperature down to 160 K, ν_Q and η grow monotonously as shown in Fig. 2. This thermal variation in the EFG parameters can be ascribed to a gradual decrease in the orthorhombic lattice parameters accompanied by a subtle increase in the Mn-O-Mn bond angle.[20] Below 160 K, η starts to decrease whereas ν_Q shows an abnormal growth that cannot be explained by the changes in the crystal symmetry and the lattice parameters. This abnormal thermal behavior of the EFG parameters, which are controlled by the electronic charge on the $2p$ orbitals, is analyzed together with the spin-density distribution in Sec. III C.

B. Magnetic susceptibility and ^{17}O NMR shifts

1. Magnetic susceptibility

Magnetic susceptibility $\chi=M/H$ of the $CaMnO_3$ sample was measured from $T=4$ K to 350 K with a superconducting quantum interference device magnetometer (Quantum Design) in magnetic field $H=50$ kOe and in the temperature range (300–670) K with Faraday balance technique in $H=2.5$ kOe. The temperature-reversible behavior of the bulk magnetization M was confirmed at high temperature by two successive heat-cool runs showing that no loss of oxygen was observed.[10] The set of $\chi(T)$ data collected with different H is presented in Fig. 3(a). Above $T_N=123(1)$ K, χ follows the Curie-Weiss law $\chi(T)\sim(T-\theta)^{-1}$ with $\theta=-380(20)$ K. The T-independent part of the magnetic susceptibility $\chi_0=0.1$ memu/mol is negligible in accordance with the corresponding χ_0 estimated in Ref. 10. The almost linear plot $\chi^{-1}(T)=H/M(T)$ shows that the mean-field behavior holds down to T_N. The linear fit shown by the solid line in Fig. 3(a) yields an effective magnetic moment $\mu_{\text{eff}}=3.9(4)\mu_B$ per Mn close to the expected value for $Mn^{4+}(S=3/2, L=0)$ ion in the cubic crystal field with half-filled t_{2g} orbitals. Thus in the PM phase, the bulk magnetization is almost completely due to the localized t_{2g} spins of the Mn^{4+} ion. The behavior of χ does not evidence any precursor of the static FM/AF inhomogeneities which appear in the sample below T_N.[8]

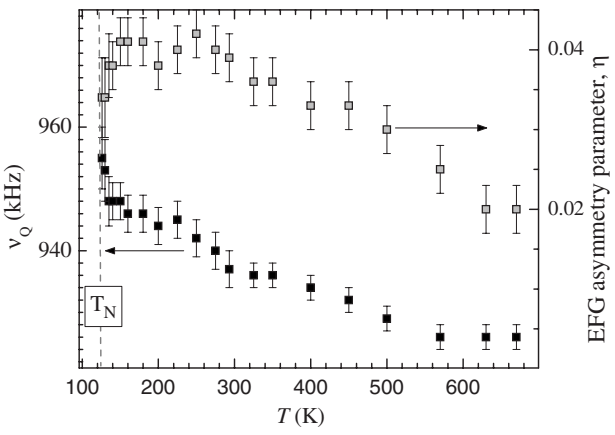

FIG. 2. Thermal behavior of the quadrupole frequency, ν_Q, and EFG asymmetry parameter, η, at the O2 site in the paramagnetic phase of $CaMnO_{3-x}$.

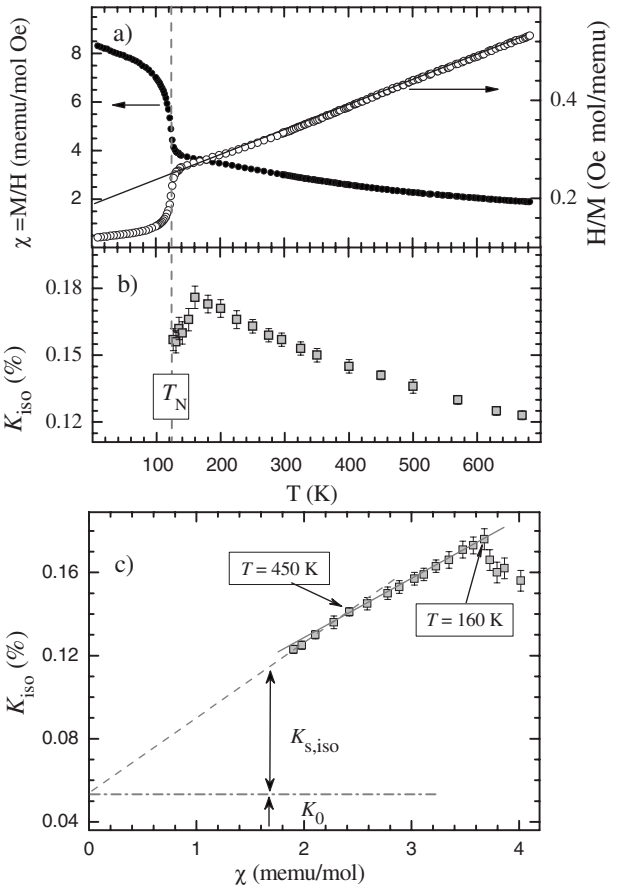

FIG. 3. (a) Magnetic susceptibility $\chi=M/H$ and (b) isotropic ^{17}O NMR shift K_{iso} versus temperature T. The straight line in (a) is a linear fit to H/M data in the PM phase. The vertical dashed line indicates the transition temperature T_N. (c) K_{iso} vs $\chi(T)$ plot with T as an implicit parameter. The solid and dashed lines are linear fits to the data below and above 450 K, respectively.

2. ^{17}O *NMR isotropic shift*

Figure 4 shows representative ^{17}O NMR spectra measured at different T and plotted versus $K \equiv (\nu - \nu_0)/\nu_0$. The width and asymmetry of the central $(m_I = +1/2 \leftrightarrow -1/2)$ transition depend on the relative values of the magnetic shift components $\{K_X; K_Y; K_Z\}$ while the position is mainly defined by the isotropic shift $K_{iso} = 1/3\{K_X + K_Y + K_Z\}$. The isotropic and anisotropic shift components were deduced from the spectra and their thermal behavior is analyzed from T_N to 670 K.

As seen in Fig. 3(b), the thermal dependence of K_{iso} evidences two distinct behaviors above and below $T \sim 160$ K. Above 160 K, the isotropic shift value decreases with the same curvature as the bulk magnetic susceptibility when T increases. Indeed, the K_{iso} versus $\chi(T)$ plot presented in Fig. 3(c) is almost linear with a slightly different slope $\Delta K/\Delta\chi$ above and below $T \sim 450$ K. For $T > 450$ K, the extrapolation of the linear fit to $\chi = 0$ (dashed line) separates K_{iso} in two parts,

$$K_{iso}(T) = K_0 + K_{s,iso}(T). \tag{1}$$

The value of $K_0 = 0.055(6)\%$ is in the range of the ^{17}O NMR chemical shifts typically observed in insulating transition-metal oxides.[25]

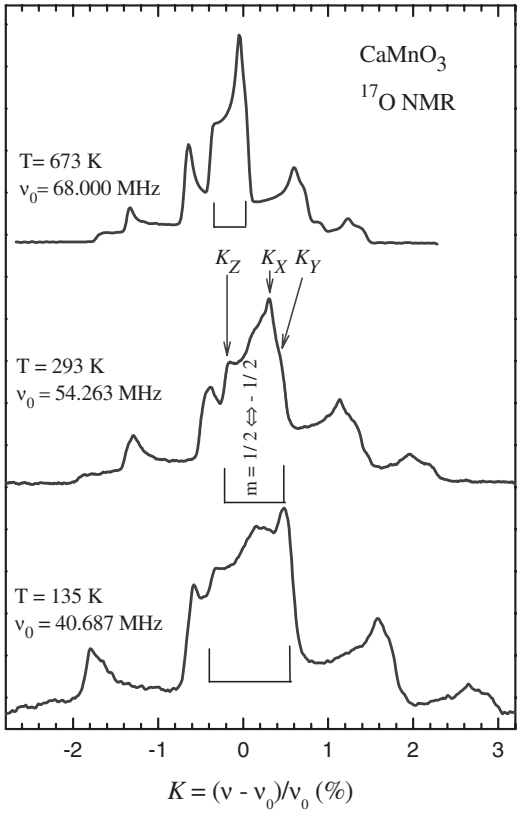

FIG. 4. Magnetic broadening of the central transition $m_I = 1/2 \leftrightarrow -1/2$ due to the magnetic shift components $\{K_X; K_Y; K_Z\}$ indicated by arrows in the ^{17}O NMR spectra versus temperature.

The temperature-dependent component $K_{s,iso}(T)$ involves the O($2s$) orbital. For this O orbital, the only possibility of a transfer of spin density from Mn electron spin is through e_g orbitals. We assume that in the PM phase, the e_g carriers may become itinerant[4] in the conducting O($2s2p_\sigma$)-Mn(e_g) band.[9] During a hop through the O($2s2p_\sigma$)-Mn(e_g) orbitals, the strong Hund coupling $-Js(e_g)S(t_{2g})$ favors the mobile e_g spin and the core t_{2g} spin to be ferromagnetically aligned. Considering the doped carriers as a Fermi gas with an effective mass $m^* = 4m_e$,[26] the corresponding uniform polarization $\langle s_z \rangle$ can be described as[27]

$$\langle s_z \rangle = g_s(E_F) J \langle S_z(t_{2g}) \rangle, \tag{2}$$

where $J > 0$ is the $q = 0$ Fourier component of the exchange coupling constant, $g_s(E_F) = (2m^* r^3_{Mn\text{-}O}/3\hbar^2) n^{1/3}$ is the carriers partial density of states of O($2s$) orbital near the Fermi level, and n is the concentration of carriers per volume unit. The corresponding local field $h_{loc}(2s)$ at oxygen site originates from the Fermi-contact interaction of the nuclear spin with the s-spin density transferred from the e_g electrons,[8,28]

$$h_{loc}(2s) = 2H_{FC}(2s)\langle s_z \rangle = 2H_{FC}(2s) g(E_F) J \langle S_z(t_{2g}) \rangle, \tag{3a}$$

$$K_{s,iso}(T) = h_{loc}(2s)/H, \tag{3b}$$

where $H_{FC}(2s) \equiv (8\pi/3)\mu_B |\phi_{2s}(0)|^2 = 1.1$ MOe (Ref. 29) is the hyperfine magnetic field due to the Fermi-contact inter-

action with one unpaired electron, the factor 2 in $h_{\rm loc}(2s)$ takes into account the two first Mn neighbors, and H is the magnetic field. As $K_{s,\rm iso}(T)$ depends on $\langle S_z(t_{2g})\rangle$, it should display in the PM phase the mean-field behavior with the same θ value as the bulk magnetic susceptibility. This is consistent with our experimental finding for $T>160$ K.

As shown in Fig. 3(c), the proportionality of the local spin density to $\chi(T)$ is broken below 160 K. According to Eqs. (3a) and (3b), a drop of $K_{s,\rm iso}(T)$ can occur only due to a drop of $g(E_F)$ and thus a decrease in n as if the carrier density diminishes in the lattice of Mn^{4+} ions when approaching T_N. In the absence of any structural changes, the decrease in $K_{s,\rm iso}(T)$ indicates that below 160 K, there are probably two kinds of doped electrons: some of the carriers contribute no more to $K_{s,\rm iso}(T)$ and $g(E_F)$. Their relative number increases when approaching T_N. We believe that below $T\sim 160$ K, these doped electrons start to be involved in strong correlations with localized Mn spins and form the magnetic polarons which are evidenced in the AF phase of the sample.[8] Being involved in strong ferromagnetic correlations, the motion of these doped electrons is much slower than that for the remaining carriers. Furthermore, they produce a very different local field at ^{17}O nuclei that shifts the resonance frequency far above the window where the ^{17}O lines shown in Fig. 1 are detected.

3. ^{17}O *NMR anisotropic magnetic shift and spin-density transfer from Mn ions*

The anisotropic magnetic shift $\{K_\alpha - K_{\rm iso}\}$ $(\alpha=X,Y,Z)$ is due to local fields produced at the ^{17}O nuclei by dipole-dipole interaction with local moments of the Mn^{4+} ions, $h_{\rm dip}$, and by anisotropic hyperfine interaction, $h_{\rm hf}$,[30]

$$(K_\alpha - K_{\rm iso})H = h_{{\rm dip},\alpha} + h_{{\rm hf},\alpha} \quad (\alpha = X,Y,Z). \tag{4}$$

For our powder sample, the components of the anisotropic magnetic shift were determined in the EFG reference system, XYZ. At the O(2) site, OZ axis is nearly parallel to $\boldsymbol{r}_{\rm Mn\text{-}Mn}$. The calculated angle, β, between OZ and $\boldsymbol{r}_{\rm Mn\text{-}Mn}$ is less than 4° (Table I) while the OX and OY EFG axes are parallel to the corresponding $\boldsymbol{r}_{\rm O2\text{-}Ca}$ vectors.

The dipolar field $h_{{\rm dip},\alpha}$ was calculated at each temperature with the static magnetic moment of Mn^{4+} ions defined as $m=\chi_{\rm mol}(T)H/N_{\rm A}$ and the α direction along H. The interatomic distances $r(\mathrm{Mn}_i\text{-O})$ were taken from the room-temperature x-ray data ignoring the small temperature variation in the PM phase.[20] Then the differences $(K_\alpha - K_{\rm iso} - h_{{\rm dip},\alpha}/H)$ enable to deduce the anisotropic hyperfine shift components $K_{{\rm hf},\alpha}=h_{{\rm hf},\alpha}/H$. We find that $|h_{{\rm hf},\alpha}|$ is about three times larger than $|h_{{\rm dip},\alpha}|$.

The anisotropic hyperfine interaction involves $O(2p_\alpha)$ orbitals. The shift components $K_{{\rm hf},\alpha}$ are plotted versus T in Fig. 5. When T decreases to about 160 K, $|K_{{\rm hf},\alpha}|$ increases following the Curie-Weiss law $K_{{\rm hf},\alpha}\sim(T-\theta_\alpha)^{-1}$, where θ_α is the fitting parameter indicated in Fig. 5. Within our accuracy, all θ_α values coincide with θ of the bulk magnetic susceptibility showing that $K_{{\rm hf},\alpha}$ also probes the t_{2g} spin polarization.

In the tight-binding approximation, the magnetic shift tensor $\{K_{{\rm hf},X};K_{{\rm hf},Y};K_{{\rm hf},Z}\}$ may be expressed with the spin density, $f_\alpha\langle S_z(t_{2g})\rangle$, transferred on $O(2p_\alpha)$ orbitals from the neighboring Mn ion[30] as

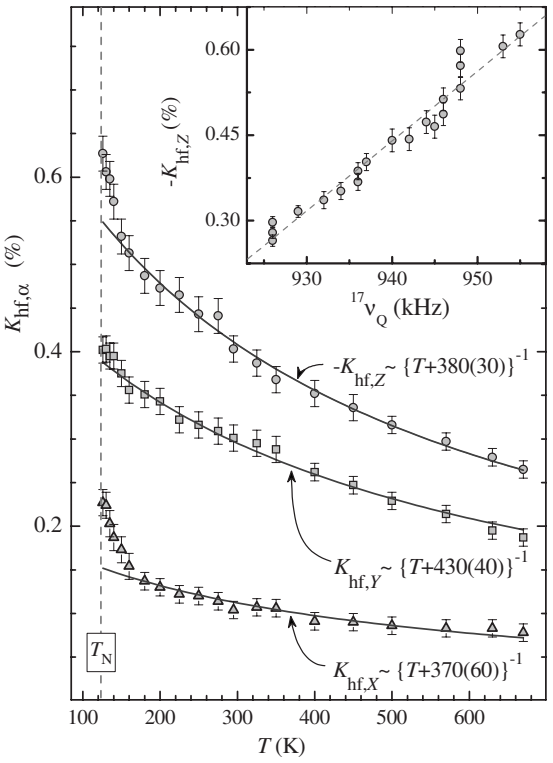

FIG. 5. Thermal dependence of the hyperfine magnetic shift components $\{K_{{\rm hf},X};K_{{\rm hf},Y};K_{{\rm hf},Z}\}$ in $CaMnO_{3-x}$. The solid curves are fitting to $K_{{\rm hf},\alpha}\sim(T-\theta_\alpha)^{-1}$, where θ_α is an adjustable parameter. Inset: $|K_{{\rm hf},Z}(T)|$ versus $\nu_Q(T)$, T being an implicit parameter.

$$K_{{\rm hf},X}H = 2\frac{2}{5}\mu_{\rm B}\langle r^{-3}\rangle_{2p}\langle S_z(t_{2g})\rangle\{-f_\sigma - f_{\pi 2} + 2f_{\pi 1}\}, \tag{5a}$$

$$K_{{\rm hf},Y}H = 2\frac{2}{5}\mu_{\rm B}\langle r^{-3}\rangle_{2p}\langle S_z(t_{2g})\rangle\{-f_\sigma - f_{\pi 1} + 2f_{\pi 2}\}, \tag{5b}$$

$$K_{{\rm hf},Z}H = 2\frac{2}{5}\mu_{\rm B}\langle r^{-3}\rangle_{2p}\langle S_z(t_{2g})\rangle\{2f_\sigma - f_{\pi 1} - f_{\pi 2}\}. \tag{5c}$$

The spin densities $f_{\pi 1,\pi 2}\langle S_z(t_{2g})\rangle$ correspond to core t_{2g} spins. This transfer results from the direct overlap of $2p_X(\pi 1)$ $[2p_Y(\pi 2)]$ oxygen orbital with d_{XZ} $[d_{YZ}]$ orbital of Mn^{4+} neighbors.[39] For f_σ, we still assume as in the case of $K_{s,\rm iso}(T)$ that the mobile e_g electrons hop through the hybridized $O(2s2p_\sigma)$-$\mathrm{Mn}(e_g)$ orbitals. These hops yield on $2p_Z\equiv 2p_\sigma$ orbitals a spin density $f_\sigma\langle S_z(t_{2g})\rangle$, where $f_\sigma = c g_s(E_F) J \sim n^{1/3}$. The factor c takes into account the ratio of the partial densities of $2s$ and $2p$ states at E_F.

The analysis of $K_{{\rm hf},\alpha}$ with Eqs. (5a)–(5c) yields $f_{\pi 2}\approx 1.3(2) f_{\pi 1}$ and $f_{\pi 2}, f_{\pi 1} \gg f_\sigma$. The nonequality of $f_{\pi 1}$ and $f_{\pi 2}$ is consistent with the orthorhombic structure whereas the strong inequality is expected for a lightly electron-doped $CaMnO_{3-x}$ sample. In the limit $x\to 0$, our estimate $(f_{\pi 2})_{\max} = 0.09(2)$ indicates a significant covalent character of the $O(2p_Y)$-$\mathrm{Mn}(d_{YZ})$ chemical bond. The lobes of the involved

orbitals are pointing toward the Ca^{2+} ion. The $Mn(t_{2g})$-$O(2p_\pi)$ hybridization was considered as an additional channel for the Mn-Mn superexchange interaction in theoretical studies.[31–34] We show that this independent channel for the superexchange interaction is anisotropic since $f_{\pi 2} \neq f_{\pi 1}$.

Below $T \sim 160$ K, the thermal behavior of $K_{\mathrm{hf},\alpha}$ deviates from the mean-field behavior (Fig. 5). The ratio, c, of the partial densities on $2s$ and $2p$ states at E_F can be evaluated at T_N. For each shift component, $K_{\mathrm{hf},Z}$ and K_{iso}, we define the difference $\Delta K = K_{\mathrm{extr}}(T_N) - K(T_N)$ between the shift value extrapolated with the mean-field behavior, $K_{\mathrm{extr}}(T_N)$, and the experimental value, $K(T_N)$. By comparing $\Delta K_{\mathrm{hf},Z}$ and ΔK_{iso}, the estimate is $c \sim 4$. Thus the spin density on $O(2p_\sigma)$ orbitals is about four times larger than on the $O(2s)$ orbital.

As the deviation from the mean-field behavior of $K_{\mathrm{hf},Z}(T)$ and $K_{\mathrm{iso}}(T)$ are detected at about the same temperature, they may have the same origin. Thus the behavior of $K_{\mathrm{hf},Z}(T)$ can be reasonably attributed to a decrease in $f_\sigma \sim n^{1/3}$ indicating a decrease in the number of itinerant electrons to the benefit of electrons involved in strong correlations when approaching the PM-AF transition.

One important result of this work concerns the comparison of $|K_{\mathrm{hf},Z}(T)|$ and $\nu_Q(T)$ shown in the inset of Fig. 5. From 500 K to T_N, the parametric plot $|K_{\mathrm{hf},Z}(T)|$ versus $\nu_Q(T)$ is well approximated by a linear dependence in spite of the fact that both $K_{\mathrm{hf},Z}(T)$ and $\nu_Q(T)$ demonstrate an unusual behavior below $T \sim 160$ K. Furthermore, $K_{\mathrm{hf},Z}$ relates to the spin density transferred from Mn to O orbitals whereas ν_Q depends on the local charge environment of oxygen nuclei. The values of ν_Q and η may be expressed in terms of the oxygen occupancies n_σ as

$$\nu_Q = \frac{3e^2Q}{20h}\langle r^{-3}\rangle_{2p}|2n_\sigma - n_{\pi 1} - n_{\pi 2}|, \tag{6a}$$

$$\eta = \left|\frac{n_{\pi 1} - n_{\pi 2}}{2n_\sigma - n_{\pi 1} - n_{\pi 2}}\right|, \tag{6b}$$

where $n_\sigma = 2\int^{E_F} g\sigma(E)dE$ and g_σ is the density of O $2p_\sigma$ states.

The proportionality found between $K_{\mathrm{hf},Z}(T)$ and $\nu_Q(T)$ data is supported by the similar form of Eqs. (5c) and (6a). Indeed, the magnetic shift data show a decrease in $f_\sigma = g_\sigma(E_F)$ below 160 K. This loss of density of states near E_F induces a decrease in n_σ. Thus the abnormal growth of ν_Q as well as the decrease in η previously described when approaching T_N are well explained by a decrease in n_σ if $n_\sigma < n_{\pi 1}, n_{\pi 2}$. This inequality is suggested for undoped $CaMnO_3$ by band-structure calculations[35] and those performed in this work. The calculations result that density of states at E_F is represented almost by $Mn(t_{2g})$ and $O(2p_\pi)$ states whereas the e_g states form the conducting band.

The proportionality between $K_{\mathrm{hf},Z}$ and ν_Q relevant, respectively, to the spin density and to the charge density transferred from the transition-metal ion to the ligand atom have a single origin associated with the semicovalent bonding between O^{2-} and Mn^{4+} ions.[36]

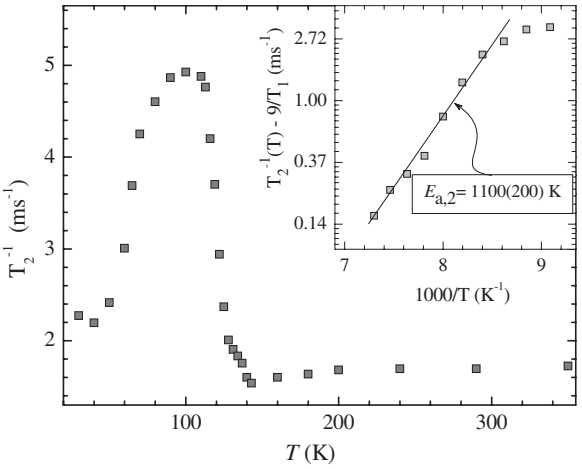

FIG. 6. ^{17}O spin-echo decay rate T_2^{-1} versus T measured in PM and AF phases of $CaMnO_{3-x}$. Inset: activated component $[T_2^{-1}(T) - 9T_1^{-1}(T)]$ versus $1000/T$. The solid line is a linear fit.

C. Dynamics of the magnetic polarons

The low-frequency dynamics of the Mn spins was probed by measuring the ^{17}O spin-echo decay rate, T_2^{-1}, on the central peak of NMR line. The thermal dependence of T_2^{-1} is displayed in Fig. 6. It shows a maximum at ~ 100 K with an almost constant behavior above 150 K.

T_2^{-1} probes the time-dependent fluctuations of the local field h at ^{17}O nuclei. The transverse and longitudinal components, $h_\perp$ and $h_\parallel$, are defined as a function of the direction of H. In general, both $h_\perp$ and $h_\parallel$ contribute to the echo-decay process,[37]

$$T_2^{-1}(T) = {}^{17}\gamma^2 h_\parallel^2 \tau_c + ({}^{17}I + 1/2)^2 T_1^{-1}(T), \tag{7}$$

where the nuclear spin-lattice relaxation rate, T_1^{-1}, involves only the transverse components thus probing $\langle h_\perp(0)h_\perp(t)\rangle$. The main contribution to the difference $(T_2^{-1})_a = [T_2^{-1}(T) - 9T_1^{-1}(T)]$ is $\langle h_\parallel(0)h_\parallel(t)\rangle = h_\parallel(0)^2 \exp(-t/\tau_c)$. Its determination requires T_1 measurements.

In the AF phase below 100 K where magnetic polarons are detected, (T_2^{-1}) probes only $\langle h_\parallel(0)h_\parallel(t)\rangle$ since the second term in Eq. (7) is found negligible. T_2^{-1} shows a thermally activated behavior with an energy barrier between the trapped and the moving magnetic polaron states $E_{a,1} = 180(20)$ K.[8] The magnetic polaron starts to move above 40 K.

In the PM phase, T_1^{-1} is found almost constant down to T_N whereas T_2^{-1} is constant down to $T \sim 140$ K and then starts to increase. As can be seen from Eq. (7), an increase in $(T_2^{-1})_a$ is due to an increase in τ_c, the correlation time characterizing the fluctuations of $h_\parallel(t)$ at O site. Above 100 K, $(T_2^{-1})_a$ has an exponential behavior versus $1/T$ (inset in Fig. 6). Assuming that the temperature dependence of τ_c is an Arrhenius law $\tau_c = \tau_{c0} \exp(E_{a,2}/T)$, we deduce $E_{a,2} = 1100(200)$ K $\gg E_{a,1}$, defining an energy scale different from the low-temperature one. Transport measurements reported for the PM phase of a nearly stochiometric $CaMnO_3$ sample yield an activation energy $E \sim 1000$ K for resistivity[4] and Hall coefficient.[11] The activation energy E was attributed to a decrease in mobility

rather than carrier density.[38] The proximity of $E_{a,2}$ and E energy barriers allows to consider that the growth of $(T_2^{-1})_a$ is caused by electrons with slower hopping.

IV. CONCLUSION

The distribution of spin and charge densities in the paramagnetic phase of a lightly electron-doped $CaMnO_{3-x}$ ($x<0.01$, $T_N=123$ K) ceramic was studied by ^{17}O NMR. It is shown that the isotropic and anisotropic components of the NMR line shift are determined by magnetic hyperfine interaction of the ^{17}O nuclear spin with the electron environment. This allows probing selectively the local spin susceptibility of the itinerant (e_g) and the localized (t_{2g}) electron of the Mn neighbors whereas the nuclear quadrupole parameters of the spectrum look at the distribution of charge density along the Mn-O bond.

Above about 160 K, the spin density of the itinerant electrons is equally shared between manganese Mn^{4+} ions. Below 160 K, the local spin density of carriers probed by ^{17}I spin in the regular lattice of the Mn^{4+} ions diminishes as approaching T_N. The density of doped electrons becomes inhomogeneously distributed since some of the electrons start to be involved in strong correlations with the localized Mn spins. Thus, according to NMR results a separation of the doped electrons into slow carriers, forming the magnetic polarons, and fast carriers develops few tens of degrees above T_N.

According to the ^{17}O echo decay-rate data, the FM-dressed electrons become unstable with increasing temperature. Their rate of hopping changes and approaches the metallic-like. The energy barrier required to excite these electrons into the O($2s2p$)-Mn(e_g) conducting band is estimated as $E_a=1100(200)$ K. Nevertheless, on the basis of ^{17}O NMR data sensitive to low-frequency spin dynamic of the mobile carriers, we cannot define in what degree their mobility at elevated temperature approaches the one existing in conducting band of a metal.

Besides, ^{17}O NMR shows directly that Mn t_{2g} electrons hybridize with the O($2p_\pi$) orbitals. This hybridization provides an independent channel for the Mn-Mn superexchange interaction. Furthermore, the thermal behavior of the anisotropic hyperfine magnetic shift and EFG parameters are correlated down to T_N. The proportionality of these properties relevant, respectively, to the spin density and the charge density transferred from transition-metal ion to the ligand atom is associated with semicovalent bonding of the $2p_\pi$ oxygen orbitals with the t_{2g} manganese ones. This correlation between charge and spin densities at the oxygen thus favors to consider the ground state of the parent $CaMnO_3$ as a charge-transfer insulator state.

ACKNOWLEDGMENTS

We are grateful to P. Monod for his help with SQUID equipment and useful discussions. This work is supported in part by the Russian Foundation for Basic Research (Grants No. 08-02-00029 and No. 09-02-00310). S.V., A.G., and A.Y. are grateful to ESPCI and CNRS for hospitality and support.

[1] M. Hennion, F. Moussa, G. Biotteau, J. Rodríguez-Carvajal, L. Pinsard, and A. Revcolevschi, Phys. Rev. B **61**, 9513 (2000).
[2] H. Terashita and J. J. Neumeier, Phys. Rev. B **71**, 134402 (2005).
[3] J. J. Neumeier and J. L. Cohn, Phys. Rev. B **61**, 14319 (2000).
[4] C. Chiorescu, J. L. Cohn, and J. J. Neumeier, Phys. Rev. B **76**, 020404(R) (2007).
[5] A. Maignan, C. Martin, F. Damay, B. Raveau, and J. Hejtmànek, Phys. Rev. B **58**, 2758 (1998).
[6] M. B. Salamon and M. Jaime, Rev. Mod. Phys. **73**, 583 (2001).
[7] E. Granado, C. D. Ling, J. J. Neumeier, J. W. Lynn, and D. N. Argyriou, Phys. Rev. B **68**, 134440 (2003).
[8] A. Trokiner, S. Verkhovskii, A. Yakubovskii, A. Gerashenko, P. Monod, K. Kumagai, K. Mikhalev, A. Buzlukov, Z. Litvinova, O. Gorbenko, A. Kaul, and M. Kartavtzeva, Phys. Rev. B **79**, 214414 (2009).
[9] H. Meskine and S. Satpathy, J. Phys.: Condens. Matter **17**, 1889 (2005).
[10] J. A. Souza, J. J. Neumeier, R. K. Bollinger, B. McGuire, C. A. M. dos Santos, and H. Terashita, Phys. Rev. B **76**, 024407 (2007).
[11] J. L. Cohn, C. Chiorescu, and J. J. Neumeier, Phys. Rev. B **72**, 024422 (2005).
[12] C. Chiorescu, J. J. Neumeier, and J. L. Cohn, Phys. Rev. Lett. **101**, 257202 (2008).
[13] E. Granado, N. O. Moreno, H. Martinho, A. Garcìa, J. A. Sanjurjo, I. Torriani, C. Rettori, J. J. Neumeier, and S. B. Oseroff, Phys. Rev. Lett. **86**, 5385 (2001).
[14] R. P. Feynman, Phys. Rev. **97**, 660 (1955).
[15] Z. Zeng, M. Greenblatt, and M. Croft, Phys. Rev. B **59**, 8784 (1999).
[16] B. Dabrowski, O. Chmaissem, J. Mais, S. Kolesnik, J. D. Jorgensen, and S. Short, J. Solid State Chem. **170**, 154 (2003).
[17] O. Chmaissem, B. Dabrowski, S. Kolesnik, J. Mais, D. E. Brown, R. Kruk, P. Prior, B. Pyles, and J. D. Jorgensen, Phys. Rev. B **64**, 134412 (2001).
[18] K. R. Poeppelmeier, M. E. Leonowicz, J. C. Scanlon, J. M. Longo, and W. B. Yelon, J. Solid State Chem. **45**, 71 (1982).
[19] I. D. Fawcett, J. E. Sunstrom, M. Greenblatt, M. Croft, and K. V. Ramanujachary, Chem. Mater. **10**, 3643 (1998).
[20] Y. Moritomo, A. Machida, E. Nishibori, M. Takata, and M. Sakata, Phys. Rev. B **64**, 214409 (2001).
[21] I. El-Kassab, A. M. Ahmed, P. Mandal, K. Bearner, A. Kattwinkel, and U. Sondermann, Physica B **305**, 233 (2001).
[22] P. Blaha, K. Schwarz, P. Sorantin, and S. B. Trickey, Comput. Phys. Commun. **59**, 399 (1990).
[23] H. Chihara and N. Nakamura, in *Nuclear Quadrupole Resonance Spectroscopy Data*, Landolt-Börnstein, New Series, Group III Vol. 20, Pt. A, edited by O. Madelung (Springer-Verlag, Berlin, 1984).

[24] J. Goodenough, Phys. Rev. **164**, 785 (1967).
[25] W. G. Klemperer, Angew. Chem., Int. Ed. Engl. **17**, 246 (1978).
[26] J. L. Cohn, M. Peterca, and J. J. Neumeier, Phys. Rev. B **70**, 214433 (2004).
[27] A. Narath, in *Hyperfine Interactions*, edited by A. J. Freeman and R. B. Frankel (Academic Press, New York, 1967), p. 415.
[28] A. Yakubovskii, A. Trokiner, S. Verkhovskii, A. Gerashenko, and D. Khomskii, Phys. Rev. B **67**, 064414 (2003).
[29] S. Fraga, J. Karwowski, and K. M. S. Saxena, *Handbook of Atomic Data* (Elsevier Scientific, Amsterdam, 1976).
[30] E. A. Turov and M. P. Petrov, *Nuclear Magnetic Resonance in Ferro- and Antiferromagnets* (Halsded Press, New York, 1972), p. 207.
[31] A. J. Millis, Phys. Rev. B **55**, 6405 (1997).
[32] H. Meskine, H. König, and S. Satpaphy, Phys. Rev. B **64**, 094433 (2001).
[33] M. Nicastro and C. H. Patterson, Phys. Rev. B **65**, 205111 (2002).
[34] J.-S. Zhou and J. B. Goodenough, Phys. Rev. B **66**, 052401 (2002).
[35] C. Cardoso, R. P. Borges, T. Gasche, and M. Godinho, J. Phys.: Condens. Matter **20**, 035202 (2008).
[36] J. Goodenough, Phys. Rev. **100**, 564 (1955).
[37] C. P. Slichter, *Principles of Magnetic Resonance* (Springer-Verlag, Berlin, 1990), p. 640.
[38] C. Chiorescu, J. J. Neumeier, and J. L. Cohn, Phys. Rev. B **73**, 014406 (2006).
[39] As the nondiagonal corrections $\sim\sin^2(\widehat{\text{Mn-O-Mn}})$ due to bending of the Mn-O-Mn bond in the orthorhombic structure of $CaMnO_3$ are small, they are ignored in Eqs. (5a)–(5c) for simplicity without loss of generality.